Evolution of surface velocities and ice discharge of Larsen B outlet glaciers from 1995 to 2013

J. Wuite[1] *, H. Rott[1, 2], M. Hetzenecker[1], D. Floricioiu[3], J. De Rydt[4], G. H. Gudmundsson[4], T. Nagler[1], M. Kern[5]

[1] ENVEO IT GmbH, Innsbruck, Austria

[2] Institute for Meteorology and Geophysics, University of Innsbruck, Austria

[3] Institute for Remote Sensing Technology, German Aerospace Center, Oberpfaffenhofen, Germany

[4] British Antarctic Survey, Cambridge, UK

[5] ESA-ESTEC, Noordwijk, the Netherlands

* Correspondence to: Jan.Wuite@enveo.at

16   **Abstract**

17

18   We use repeat-pass SAR data to produce detailed maps of surface motion covering the glaciers

19   draining into the former Larsen B Ice Shelf, Antarctic Peninsula, for different epochs between 1995

20   and 2013. We combine the velocity maps with estimates of ice thickness to analyze fluctuations of

21   ice discharge. The collapse of the central and northern sections of the ice shelf in 2002 led to a near-

22   immediate acceleration of tributary glaciers as well as of the remnant ice shelf in SCAR Inlet.

23   Velocities of most of the glaciers discharging directly into the ocean remain to date well above the

24   velocities of the pre-collapse period. The response of individual glaciers differs and velocities show

25   significant temporal fluctuations, implying major variations in ice discharge as well. Due to reduced

26   velocity and ice thickness the ice discharge of Crane Glacier decreased from 5.02 Gt a^{-1} in 2007 to

27   1.72 Gt a^{-1} in 2013, whereas Hektoria and Green glaciers continue to show large temporal

28   fluctuations in response to successive stages of frontal retreat. The velocity on SCAR Inlet ice shelf

29   increased two- to three fold since 1995, with the largest increase in the first years after the break-up

30   of the main section of Larsen B. Flask and Leppard glaciers, the largest tributaries to SCAR Inlet

31   ice shelf, accelerated. In 2013 their discharge was 38 % and 46% higher than in 1995.

32

1. Introduction

Atmospheric warming and changes in ocean conditions during the past decades led to wide-spread retreat of ice shelves around the Antarctic Peninsula (API) (Cook and Vaughan, 2010). Progressive retreat culminated in the final disintegration of the Larsen A ice shelf in January 1995 and of the northern and central sections of the Larsen B Ice Shelf in March 2002 (Rott et al., 1996; Rack and Rott, 2004; Glasser and Scambos, 2008). The glaciers flowing from the Antarctic Peninsula plateau, previously feeding the ice shelves, became tidewater glaciers. Most of these glaciers accelerated significantly, resulting in increased ice discharge (Rott et al., 2002; De Angelis and Skvarca, 2003; Rignot et al., 2004; Scambos et al., 2004). The response of these glaciers to ice-shelf disintegration is of particular interest not only for quantifying the contributions of API outlet glaciers to sea level rise, but also for studying processes of ice shelf retreat and its interactions with grounded ice (Vieli and Payne, 2005; Hulbe et al., 2008).

Investigations on retreat and acceleration of glaciers in the Larsen Ice Shelf region so far focused mainly on the Larsen B embayment. Rignot et al. (2004) and Scambos et al. (2004) reported on acceleration of main glaciers draining into the Larsen B embayment, based on analysis of satellite images. Rott et al. (2011) derived velocities of nine Larsen B glaciers in pre-collapse state and in 2008 and 2009 from high-resolution radar images, and estimated calving fluxes and mass balance. Estimates of the mass balance of Larsen B glaciers in recent years have been derived from changes in surface topography. Shuman et al. (2011) and Scambos et al. (2011) tracked elevation changes over the period 2001 to 2009 using optical stereo imagery and laser altimetry of ICESat and of the airborne ATM sensor. Shuman et al. (2011) reported a combined mass loss of 8.4 Gt a^{-1} for these glaciers for the period 2001 to 2006, excluding ice lost by frontal retreat. Berthier et al. (2012) explained that the mass loss of former Larsen B tributary glaciers continued at almost the same rate over the period 2002 to 2011, reporting a mass loss rate of 9.04 Gt a^{-1} for the period 2006 to 2010/2011. Scambos et al. (2014) used satellite laser altimetry and satellite stereo-imagery to map ice elevation change and inferred mass changes for 33 glacier basins of the northern API over the time span 2001-2010. They report a mass balance of -7.9 Gt a^{-1} for the tributaries to the Larsen B embayment and -1.4 Gt a^{-1} for the tributaries to the remnant ice shelf in SCAR Inlet.

These reports provide estimates of mass depletion for the Larsen B tributaries integrated over multi-year periods. Here we present new analysis of satellite data showing the spatial and temporal variability in velocities over the whole Larsen B area dating back to 1995. We have included new satellite data not used in any previous studies so far, and have also reprocessed satellite radar images to generate fully consistent and comparable data sets on surface velocities. Our work

includes both recent acquisitions by high resolution radar sensors as well as archived data, some of which have not been exploited until now. Velocity data and estimates of ice thickness are used to derive ice discharge at different epochs, showing significant temporal variability as well. The data sets provide a comprehensive basis for studying the dynamic response of the ice masses to the disintegration of Larsen B, including the glaciers that are draining now directly into the ocean as well as the remnant ice shelf in SCAR Inlet and its tributary glaciers.

2. Data and methods

We derived maps of ice flow velocities from repeat-pass Synthetic Aperture Radar (SAR) data of the satellite missions ERS-1, ERS-2, Envisat, TerraSAR-X (TSX), and ALOS, applying either offset tracking or SAR interferometry (InSAR). The source data were obtained from the archives at the European Space Agency (ESA) and the German Aerospace Center (DLR). We retrieved two-dimensional surface displacement in radar geometry which we projected onto the surface, defined by the ASTER based Antarctic Peninsula DEM (API-DEM) of Cook et al. (2012), in order to produce maps of surface velocities. The maps of the surface velocity vector are provided in Antarctic polar stereographic projection resampled to a 50 m grid. The DEM is compiled from ASTER scenes from a range of dates between 2000 and 2009 which are unspecified in the final product (Cook et al, 2012). During this period various glaciers have been subject to major drawdown. The sensitivity analysis on the impact of possible DEM errors shows that even in extreme cases of surface lowering the induced error in geocoded velocity is below 1%.

The spatial resolution of the SAR images along the flight track and in radar line-of sight (LOS) ranges from 3.3 m x 1.2 m for TSX to 5.6 m x 9.6 m for the Advanced Synthetic Aperture Radar (ASAR) of Envisat. The time span of the repeat pass image pairs ranges from one day for ERS-1/ERS-2 tandem images to 46 days for ALOS Phased Array L-band SAR (PALSAR) images. Because of temporal decorrelation of the phase of the backscatter signal the interferometric (InSAR) method could only be applied for ERS-1/ERS-2 tandem images, available on several dates of the years 1995 to 1999. InSAR data of a single swath provide the surface displacement in LOS. We combined image pairs of ascending and descending orbits to derive 2-D velocity fields for the period late 1995 to early 1996. Being well before the collapse of the Larsen B Ice Shelf, this period is of particular importance as reference for studying the impact of ice shelf disintegration on tributary glaciers. For 1999 ERS SAR data were available only from single view direction. Assuming unaltered flow direction since 1995/1996, we derived velocity maps in November 1999, using the argument from the velocity vectors of crossing orbits.

4

99   For retrieving maps of ice motion from the TSX SAR, Envisat ASAR and ALOS PALSAR we

100 apply the offset tracking technique which is based on cross-correlation of templates in SAR

101 amplitude images. Offset tracking delivers along track and LOS velocity components from a single

102 image pair. It is less sensitive to displacement than InSAR, but this drawback is (at least partly)

103 compensated by the longer time span between the repeat pass images (Rott, 2009). We used

104 templates of 64 x 64 and 96 x 96 pixels size and applied sampling steps of 10 pixels for generating

105 velocity maps. TSX images are our main data sources for velocity maps between 2007 and 2013,

106 complemented by occasionally available ALOS PALSAR data. Envisat ASAR data are the basis for

107 velocity maps for 2003 to 2006 on large glaciers and on the SCAR Inlet ice shelf.

108 The uncertainty of retrieved velocities differs between the sensors. The ERS InSAR motion maps

109 are based on InSAR pairs of good coherence. One fringe (phase cycle of 2π) corresponds to 7.2 cm

110 projected onto a horizontal surface. Assuming an uncertainty of 0.2 fringes for a point on the

111 moving glacier surface and 0.2 for the zero velocity reference points on ice free surfaces, for ERS

112 InSAR the uncertainty in surface velocity of grounded ice is ±0.02 m d^{-1}. On floating ice control

113 points without horizontal motion are used as reference, so that the observed signal corresponds to

114 the tidal displacement. The phase differences between individual reference points, located around

115 the Seal Nunataks and in inlets along Jason Peninsula, are less than 0.5 fringes. Assuming an

116 uncertainty of 0.2 fringes for the moving ice shelf and of 0.5 fringes for the reference points, the

117 uncertainty in horizontal velocity of floating ice is ±0.04 m d^{-1}.

118 For offset tracking the accuracy depends on the pixel size, the time interval, and the quality of

119 features in order to obtain good correlation peaks. We excluded areas of low correlation, so that the

120 uncertainty for the retrieval of displacement is in the order of 0.2 to 0.3 pixels. The resulting

121 uncertainties in the magnitude of surface motion are ±0.05 m d^{-1} for TSX SAR, ±0.08 m d^{-1} for

122 ALOS PALSAR and ±0.15 m d^{-1} for Envisat ASAR.

123 The mass flux across a gate of width Y [m] near the calving front or grounding line is computed

124 according to:

125
$$F_Y = \rho_{ice} \int_{y=0}^{y=Y} [u_m(y) \sin\theta \, H(y)] dy \qquad (1)$$

126 Where ρ_{ice} is the density of ice, u_m is the vertically averaged horizontal velocity, θ is the angle

127 between the velocity vector and the gate, H is the ice thickness. We use a column-averaged ice

128 density of 900 kg m^{-3} to convert ice volume into mass. For calving glaciers full sliding is assumed

129 across calving fronts, so that u_m corresponds to the surface velocity, u_s, obtained from satellite data.

130 For glaciers discharging into the ice shelf we estimate the ice deformation at the flux gates applying

5

131 the laminar flow approximation (Paterson, 1994) using a rate factor as derived by Hulbe et al.
132 (2008) for outlet glaciers to Larsen-B. The results show moderate values of deformation velocities.
133 For Crane Glacier the resulting vertically averaged velocity (pre-collapse) is $u_m = 0.96 \, u_s$, for other
134 glaciers $u_m = 0.95 \, u_s$. Ice thickness at the flux gates is obtained from various sources. For Flask and
135 Starbuck glaciers radar sounding data are available (Farinotti et al., 2013; 2014). For Crane Glacier
136 the cross section of the calving gate is deduced from bathymetric data (Zgur et al., 2007; Rott et al.
137 2011). For Leppard Glacier ice thickness data of Huss and Farinotti (2014) are used. For calving
138 fluxes of Crane, Hektoria and Green glaciers the ice thickness in the centre of the flux gate is
139 estimated from surface height above sea level assuming flotation. The central sections of these
140 glacier fronts have been floating at least since 2007. The surface elevation near the calving front is
141 obtained from laser ranging data of ICESat and the Airborne Thematic Mapper (ATM) (Shuman et
142 al., 2011; Krabill and Thomas, 2013; 2014) and in 2011 and 2013 also from digital elevation data of
143 TanDEM-X (Krieger et al., 2013). For uncertainty estimates of mass fluxes through the gates we
144 assume ±10 % error of the cross section area for Starbuck, Flask and Crane glaciers, and ±20 % for
145 Hektoria, Green, Jorum and Leppard glaciers. For velocity across the gate we assume ±5 %
146 uncertainty.

147

148 **3. Evolution of glacier velocities**

149 **3.1 Velocities and frontal retreat of glaciers draining into Larsen B embayment**

150 The location of the glacier basins is shown in Fig. 1, and the areas of the basins for the region
151 upstream of the 1995 grounding line and of the 2012 glacier fronts are specified in Table 1. The
152 basin outlines inland were provided by A. Cook based on the ASTER derived Antarctic Peninsula
153 DEM (API-DEM) (Cook et al., 2012). The positions of the grounding lines in 1995 are from the
154 ERS InSAR analysis of Rack (2000). The update of glacier fronts and areas in 2012 is based on a
155 Landsat image of 12 January 2012. Before 2002 all glaciers between the Seal Nunataks and Jason
156 Peninsula drained into Larsen B Ice Shelf. Since its collapse, in March 2002, they drain into a wide
157 bay and in the remnant part of the ice shelf in SCAR Inlet. The area of the Larsen B tributary
158 glaciers decreased by 270 km^2 since 1995. The 2012 area refers to the ice front rather than the
159 grounding line, so that the total loss in grounded ice extent is slightly higher because frontal
160 sections of some glaciers are floating.

161 The largest glaciers north of SCAR Inlet, where the ice shelf disappeared in 2002, are Hektoria-
162 Green-Evans (HGE) and Crane glaciers. Before the ice shelf breakup the frontal zone of HGE
163 glaciers was formed by the confluence of the three glaciers, stretching across a wide bay. Following

6

the ice shelf collapse the frontal regions of HGE retreated quickly (Rack and Rott, 2004; Scambos et al., 2004), suggesting that they were lightly grounded and sensitive to changes in ice-shelf buttressing. The ice shelf collapse resulted in the progressive breakup of increasingly large areas of grounded ice concomitant with acceleration of ice flow and dynamic thinning, amounting to a total retreat of 174 km^2 by January 2012. On Crane Glacier the loss of grounded ice has been smaller (35 km^2) because the terminus is confined in a narrow fjord. Jorum Glacier lost 24 km^2 in grounded ice, Punchbowl Glacier 12 km^2, and Melville Glacier 4.1 km^2. The frontal positions of Mapple and Pequod glaciers have been stationary.

An overview map of surface velocities for the Larsen B region is shown in Fig. 2a for the year 1995 based on ERS InSAR data. As already reported by Rott et al. (2011), the 1995 velocities of outlet glaciers to Larsen-B agree within a few percent with the velocities retrieved from 1999 InSAR data. There is no indication for a significant temporal trend in velocity on any of the glaciers. The velocities, derived from InSAR data on various dates in 1995 and 1999 differ by less than 5 % at any of the flux gates. Varying tidal deformation along the ice shelf margins, observed in the different interferograms, did not affect the ice motion at these flux gates which are located several kilometres inland of the 1995 - 1999 grounding zone.

Fig. 2b is a composite of several velocity maps from TSX and ALOS PALSAR offset tracking analysis of the years 2008 to 2012. As the figures show, a major flow acceleration is observed for HGE, Jorum, and Crane glaciers. Flask and Leppard glaciers in SCAR Inlet also accelerated, but at a lower rate. In order to investigate the temporal evolution of velocities we extracted profiles along the central flow line of the main glaciers: Hektoria, Green, Jorum, Crane, Punchbowl and Melville glaciers, now terminating with calving fronts (Fig. 3), and Flask and Leppard which are still confined by the remnant part of Larsen B Ice Shelf. The location of the profiles is charted in Fig. 1. The map of velocity changes (Fig. 2c) and the longitudinal profiles show that the flow acceleration extends far upstream on the large glaciers, whereas on the smaller glaciers the acceleration has been modest and confined to the lower part of the tongues.

The velocity of Hektoria and Green glaciers is presently still much higher than in 1995, but has been subject to strong variations since 2002 associated with glacier thinning and frontal retreat. The velocity profiles (Fig. 3) show periods of acceleration followed by gradual deceleration. In 2008 Hektoria and Green glaciers still had a common terminal section, but the lower terminus was already heavily fractured (Fig. 4). In 2009 a major section along the front broke away leading to another rise in velocities. In November 2009 the frontal velocity of Hektoria and Green glaciers was about twice the velocity at the same point in October 2008. The high velocities persisted until March 2012, after which significant slow-down and an interim advance of the floating tongues was

7

198 observed in 2013.

199 Ice flow and calving fluxes of Crane and Jorum glaciers have been investigated by Rott et al. (2011)

200 based on ERS InSAR data of 1995 and 1999 and TerraSAR-X data of several dates between

201 October 2008 and November 2009. During 2008/09 the velocity was comparatively stable on both

202 glaciers (Rott et al., 2011). Our analysis of the extended TSX data set shows a strong deceleration

203 since 2007. The velocity in the centre of the flux gate 1 km upstream of the 2008 glacier front

204 decreased from 6.8 m d^{-1} in June 2007 to 5.2 m d^{-1} in November 2008 and October 2009, and to 2.9

205 m d^{-1} in November 2013. Between 2003 and 2007 the strong acceleration of Crane Glacier caused

206 dynamic thinning and subsidence on the order of 150 m on the lower terminus (Scambos et al.,

207 2011). In spite of continued thinning, although with reduced rate, the position of the glacier front

208 has been rather stable since 2006. The shape of the glacier bedrock in form of a deep canyon,

209 inferred from bathymetric data, indicates that the central part of the lower terminus has been

210 ungrounded for several years (Rott et al., 2011). This suggests that lateral drag plays a key role in

211 maintaining the frontal position since 2006. Also the velocity of the Jorum Glacier terminus is still

212 higher than before ice shelf collapse. As on Crane Glacier, the velocity decreased since 2007, but at

213 smaller percentage.

214 The velocities of the glaciers that are originating east of the main ice divide are small, and the flow

215 acceleration has been modest. On Punchbowl Glacier the velocity at the central flow line near the

216 calving gate increased from 0.20 m d^{-1} in 1995 to 0.50 m d^{-1} in 2008 to 2012, on Melville Glacier

217 form 0.25 m d^{-1} in 1995 to 0.40 m d^{-1} in 2008 and 0.70 m d^{-1} in 2012 (Fig. 3). Whereas Punchbowl

218 and Melville Glaciers have been subject to frontal retreat, the frontal positions of Mapple and

219 Pequod glaciers have been stable. This is reflected in the observed velocities near the front. On both

220 glaciers a temporary acceleration is observed in 2007: on Pequod Glacier from 0.29 m d^{-1} in 1995 to

221 0.40 m d^{-1} in 2007; on Mapple Glacier from 0.16 m d^{-1} in 1995 to 0.21 m d^{-1} in 2007. During the

222 period 2008 to 2012 the velocities returned to the pre-collapse values.

223 The velocity variations of the outlet glaciers are clearly dominated by multi-annual trends triggered

224 by ice shelf disintegration. On some of the glaciers seasonal variations in velocity by a few per cent

225 are observed, but not in every year. Compared to the long term trend this signal is not significant.

226 **3.2 Velocities of SCAR Inlet ice shelf and tributary glaciers**

227 The area of the ice shelf in SCAR Inlet decreased from 3463 km^2 on 18 March 2002 (Rack and

228 Rott, 2004) to 1870 km^{2}in January 2012. The velocities on the ice shelf section which is nourished

229 by Flask and Leppard glaciers increased two- to three-fold since 1995/1999. This section is

230 separated by distinct shear zones from the ice shelf sections along Jason Peninsula and the section

downstream of Starbuck and Stubb glaciers (Fig. 5). Major rifts are apparent on the ice shelf in the ASAR image of 28 January 2004, indicating that the disintegration of the main section of Larsen B Ice Shelf affected the stability of the remnant ice shelf in SCAR Inlet rather soon. In June 2004 the velocities along the central flowlines downstream of Flask and Leppard glaciers had already doubled compared to the pre-collapse values (Fig. 6), another indication that the Larsen B disintegration event had a rather immediate impact on the stress field of SCAR Inlet ice shelf. In the profiles of 1995 and 1999, based on one-day InSAR repeat pass data, we exclude the tidal deformation zone because of ambiguity between horizontal motion and vertical displacement.

In spite of still being backed up by an ice shelf, both Flask and Leppard glaciers accelerated since 1995/1999 (Fig. 6). Between 1995 and 1999 there are no apparent differences in velocity. On Flask Glacier the mean velocity in 2009 to 2013 at the flux gate, 6 km above the grounding line, is 41 % higher than the velocity in 1995/1999. On Leppard Glacier the velocity at the flux gate, 4 km above the grounding line, increased by 45 %. The signal of acceleration between the two periods extends more than 30 km up-glacier, with the velocity change decreasing with distance from the grounding zone. The acceleration of the glaciers is in line with substantial acceleration of SCAR Inlet ice shelf since 2002. The main speed-up happened before 2009. Between September 2009 and July 2013 the velocities have been rather stable. The smaller Rachel, Starbuck and Stubb glaciers do not show any significant change in velocities since 1995.

4. Temporal variations of ice discharge

Estimates of ice discharge of Crane, Jorum, Hektoria, and Green glaciers in different years are presented in Table 2. The estimated discharge of Hektoria and Green glaciers for 1995 amounts to 1.19 Gt a^{-1} using the same gate near the 2008 front as Rott et al. (2011) (Fig. 4). By February/March 2004, two years after the collapse, the maximum velocity at this gate was 5.1 m d^{-1} (1862 m a^{-1}), five times higher than in 1995. A transect on Hektoria Glacier, acquired by the NASA ATM in 2004 (Krabill and Thomas, 2013), allows for an estimate of an ice thickness of 406 m under the assumption of flotation, resulting in a flux of 4.74 Gt a^{-1}. The estimate for 2008 by Rott et al. (2011) amounts to 2.88 Gt a^{-1}. At that time the two glaciers still formed a single calving front. The maximum velocity at the front was 4.23 m d^{-1} (1545 m a^{-1}) and the maximum ice thickness at the (floating) calving gate, inferred from an ICESat profile, is estimated at 268 m. Because of the retreat of the terminus by 4 km between 2008 and 2011, the gates for the 2010 and 2013 fluxes are shifted inland (Fig. 4). A transect of surface elevation on Hektoria Glacier was measured in 2011 by the ATM during the IceBridge campaign. The freeboard at the gate is 55 m, resulting in a maximum ice thickness of 450 m assuming freely floating ice. The corresponding numbers for the calving

9

265   fluxes, with November 2010 velocities, are 1.67 Gt a^{-1}for Hektoria Glacier and 1.99 Gt a^{-1}for Green

266   Glacier, adding up to 3.66 Gt a^{-1} which is 27 % higher than the flux in 2008. By July 2013 the

267   combined flux decreased to 3.05 Gt a^{-1}. This illustrates the impact of velocity variations on calving

268   fluxes, resulting in major fluctuations of glacier net mass balance within a few years.

269   For computing the ice flux for Crane Glacier, the same flux gate 1 km inland of the ice front in

270   2008 and 2009 is used as by Rott et al. (2011) (Fig. 4). Because of slow down of ice flow (Fig. 3)

271   and reduction in ice thickness, the calving flux of Crane Glacier decreased significantly during

272   recent years. Based on the June 2007 analysis the flux across the gate is estimated at 5.02 Gt a^{-1}, 4.4

273   times higher than the pre collapse calving flux of 1.15 Gt a^{-1}. Until November 2013 it decreases to

274   1.72 Gt a^{-1}, one third of the 2007 flux.

275   In 1995 the combined mass flux of Jorum Glacier across the 2008 calving gates of the two glacier

276   branches amounted to 0.35 Gt a^{-1} (Rott et al., 2011). For 2008 the elevation data from an ICESat

277   transect close to the gates were used to estimate the maximum ice thickness. For estimating the ice

278   thickness in 2012 we use surface elevation data of the TanDEM-X satellite mission, which show

279   surface lowering by a few metres since 2008. The estimated calving flux for the two branches of

280   Jorum Glacier decreased from 0.61 Gt a^{-1} in 2008 to 0.45 Gt a^{-1} in 2013.

281   For Starbuck, Flask and Leppard glaciers data on ice thickness are available from ice sounding

282   measurements and ice flow modelling (Farinotti et al., 2013; 2014; Huss and Farinotti, 2014). On

283   Starbuck Glacier the TSX ice motion data of 2009 and 2011 do not reveal any significant difference

284   compared to 1995 (Fig. 7). Therefore the discharge has likely not changed significantly either. The

285   flux through the cross section near the grounding line, with maximum velocity of 0.34 m d^{-1} (124 m

286   a^{-1}), is estimated at 0.67 Gt a^{-1} (Table 3). The ice on Flask and Leppard glaciers is thicker and

287   velocities are higher. For Flask Glacier the mass flux is derived for a gate along a transverse profile

288   4 km above the grounding line (Fig. 7). This corresponds to the position of radio echo sounding

289   profile 1, acquired by the BAS Polarimetric Airborne Survey Instrument in November 2011

290   (Farinotti et al., 2013). In the centre of the profile the ice thickness is 690 m. In 1995 and 1999 the

291   velocities in the centre are 1.31 m d^{-1} (478 m a^{-1}) and 1.36 m d^{-1} (496 m a^{-1}) respectively, the

292   resulting ice discharge across the gates is 0.78 Gt a^{-1} and 0.80 Gt a^{-1} for the two years. On Flask

293   Glacier the velocities in 2009 to 2013 vary between 1.76 m d^{-1} (642 m a^{-1}) and 1.93 m d^{-1} (704 m a^{-1}

294    $^{-1}$), and the ice discharge ranges from 1.08 Gt a^{-1} to 1.23 Gt a^{-1}, without a clear temporal trend. The

295   discharge increased between 37 % and 56 % compared to 1995 and 1999. On Leppard Glacier the

296   centre line velocity at the gate near the grounding line has increased from 1.00 m d^{-1} (365 m a^{-1}) in

297   1995 to 1.44 m d^{-1} (526 m a^{-1}) in 2009 and 1.48 m d^{-1} (541 m a^{-1}) in 2013. The flux increased from

298   1.22 Gt a^{-1} in 1995 to 1.74 Gt a^{-1} in 2011 and 1.78 Gt a^{-1} in 2013, an increase of 43 % and 46 %,

299   respectively. As for Flask Glacier, there is no significant difference between 2009 and 2013.

300   The flow acceleration and increased ice discharge results in dynamic thinning which is confirmed

301   by ICESat laser altimeter measurements. For analysis of elevation change we selected dates with

302   closely spaced ICESat repeat tracks: track 129 of 1 June 2004 and 27 November 2008 shifted by 31

303   m on Leppard Glacier and 28 m on Flask Glacier; track 390 of 18 June 2004 and 19 March 2008

304   shifted by 71 m on Leppard Glacier. We corrected for the shift by taking into account the surface

305   slope derived from the API-DEM. For track No. 129, crossing Flask Glacier 0.5 km downstream

306   and Leppard Glacier 5 km upstream of the flux gate, we obtain a mean annual rate of surface

307   elevation change of -1.93 m a^{-1} on Leppard Glacier and of -2.22 m a^{-1} on Flask Glacier. For track

308   No. 390 we obtain for a profile across Leppard Glacier 13 km upstream of the flux gate a mean

309   annual rate of elevation change of -1.71 m a^{-1}.

310

311   **5. Discussion**

312   In line with previous studies, our data shows a drastic increase in flow velocities of major tributary

313   glaciers following the collapse of Larsen B Ice Shelf in early 2002. Reduced backstress and frontal

314   retreat caused flow acceleration that propagated up-glacier. Beyond that, our analysis of new

315   velocity data shows that some of the glaciers slowed down significantly during recent years. Strong

316   acceleration and increase of calving flux is observed for HGE glaciers and Crane Glacier,

317   downstream of which the seafloor map shows deep troughs (Lavoie et al., 2015).

318   Scambos et al. (2004) present data of ice motion in 2001, 2002, and 2003 along selected points of

319   the central flow-lines of the glaciers Crane, Jorum, Hektoria, and Green, derived by feature tracking

320   in Landsat images. They report for a point near the Hektoria Glacier front a velocity increase from 1

321   m d^{-1} in 2001 to 5 m d^{-1} in early 2003. Rignot et al. (2004) derived velocities up to 6 m d^{-1} in 2003

322   near the front of Hektoria Glacier from Radarsat images which agrees with our analysis of ASAR

323   data of December 2003. Scambos et al. (2011) derived velocities for six periods between April 2002

324   and December 2009 for a point 6 km upstream of the Crane Glacier front, showing a maximum

325   velocity of 5.3 m d^{-1} in January 2006, similar to the value of 5.5 m d^{-1} we derived for this point

326   from TSX data of June 2007.

327   Subsequently, our analysis shows significant deceleration for Crane Glacier since mid-2007, yet

328   over this time period the position of the ice front has remained comparatively stable. Possibly this is

329   due to a reduction in the ratio between driving stress and lateral shear, in accordance with

330   decreasing surface slope on the lower glacier terminus. Targeted ice-flow modelling is required to

331   further address this issue. From June 2007 to November 2013 the calving flux of Crane Glacier
332   decreased from 5.02 Gt a^{-1} to 1.72 Gt a^{-1}. Under the assumption that the pre-collapse flux
333   corresponds to the balance flux (Rott et al., 2011), the resulting rate of mass loss decreased from
334   3.87 Gt a^{-1} to 0.57 Gt a^{-1}. Based on differencing of DEMs from optical stereo imagery in
335   combination with ICESat data, Scambos et al. (2014) report a mean loss rate of 2.24 Gt a^{-1} for the
336   period March 2003 to November 2008. This is 42 % lower than our estimate for June 2007 and 35%
337   higher that our estimate for 2008/09. These large temporal variations emphasize the importance of
338   using common epochs when comparing glacier contributions to sea level rise obtained by different
339   methods.

340   Whereas on Crane Glacier a period of major flow acceleration during the first five years after ice
341   shelf disintegration was followed by a steady gradual decrease in velocity, the flow behaviour of
342   Hektoria and Green glaciers has been more variable. Periods with increased flow velocities and
343   frontal retreat alternated with periods of comparatively stable front positions or short-term advance.
344   ASTER and ICESat data show substantial elevation losses on lower Green Glacier amounting to
345   about 100 m during the time span November 2001 to late 2008 (Shuman et al., 2011). Scambos et
346   al. (2014) report for HG glaciers a mean loss rate of 3.84 Gt a^{-1} for the period March 2003 to
347   November 2008 out of which 0.53 Gt a^{-1} are attributed to the loss of ice mass above floating for the
348   retreating glacier area. Our estimate of the calving flux across the 2008/09 gate, located about 4 km
349   inland of the 2004 ice front, yields 4.74 Gt a^{-1} for March 2004 and 2.88 Gt a^{-1} for 2008/09. With the
350   estimated balance flux of 1.19 Gt a^{-1} (Rott et al., 2011), the resulting net balance for the glacier area
351   above the 2008/09 gate amounts to -3.55 Gt a^{-1} based on velocities of March 2004. For 2008 the
352   estimated net balance is -1.69 Gt a^{-1}. The loss rate increased in 2010/2011, and decreased in 2013,
353   with the discharge in Table 3 referring to gates shifted inland because of frontal retreat.

354   Hektoria, Green and Evans glaciers, forming a joined terminus in a wide bay in 2002, have been
355   particularly vulnerable to stress perturbation after ice shelf collapse as evident from the frontal
356   retreat. Successive phases of transition from weakly grounded to floating ice due to flow
357   acceleration and thinning, associated with major calving events, have been maintaining high rates of
358   mass depletion for HGE glaciers to date. Crane and Jorum glaciers, terminating in deep and narrow
359   fjords, have been subject to acceleration and major mass depletion during the first five years after
360   ice shelf collapse, but slowed down afterwards. Similar behaviour after retreat into narrow fjords is
361   observed for Sjögren-Boydell glaciers in Prince-Gustav-Channel and for Dinsmoor-Bombardier-
362   Edgeworth glaciers in the Larsen A embayment (Rott et al., 2014). The ratio of longitudinal stress to
363   lateral shear stress is critical for glacier motion in narrow valleys (Hulbe et al. 2008). Decreasing ice
364   thickness and surface slope affect driving stresses and cause deceleration in flow. However,

12

365 considering the ongoing thinning of the terminus and the resulting decrease of lateral shear stress, it
366 can be concluded that Crane and Jorum glaciers will still be subject to major retreat before reaching
367 a new equilibrium state further inland.

368 The two main glaciers draining into SCAR Inlet ice shelf, Flask and Leppard glaciers, have also
369 been affected by flow acceleration in recent years. GPS measurements at stakes on Larsen B located
370 50 km downstream of these glaciers showed flow acceleration in the order of 10 % between 1994
371 and 1999 (Rack, 2000). This indicates that also the southern sections of Larsen B Ice Shelf had
372 weakened mechanically previous to the disintegration event in 2002, as reported for the northern
373 and central sections (Rack et al., 2000; Rack and Rott, 2004). Our analysis of substantial flow
374 acceleration and development of rifts, evident in satellite data of 2004, implies that the break-up had
375 a near immediate impact on the stress field of the ice shelf. Fricker and Padman (2012) report for
376 two crossover points on SCAR Inlet ice shelf relatively constant elevation change of ~-0.19 m a^{-1}
377 during 1992 to 2008. Our analysis of the temporal evolution of ice shelf flow suggests that changes
378 in the rheology and stress field might not have been continuous during this period. The main speed-
379 up on SCAR Inlet ice shelf occurred during the first two years after the disintegration of the
380 northern and central sections of Larsen B, whereas changes later on were more gradual. Given the
381 spatial pattern of acceleration, with main speed-up in the ice shelf section nourished by Flask and
382 Leppard glaciers, further weakening has to be expected along the shear margins of this section, as
383 well as for the ice immediately downstream of the grounding zone. Numerical models of Larsen B
384 Ice Shelf in pre-collapse state show a band of weak ice along the shear zone that separates the
385 outflow of Leppard Glacier from the slowly moving ice along Jason Peninsula (Rack et al., 2000;
386 Vieli et al., 2006). The differential acceleration of flow and the formation of additional rifts, which
387 are evident in ASAR and TSX images since 2004, indicate that ice in this zone is further
388 weakening.

389 Whereas the ice at the flux gates of Leppard and Flask glaciers accelerated from 1995 to 2009 by
390 44% and 38%, respectively, the velocity of Starbuck Glacier has been stable. This can on one hand
391 be attributed to the bedrock topography, on the other hand to the rather modest mass turnover. The
392 lower terminus of Starbuck Glacier is firmly grounded, with a broad sub-glacial ridge in the area of
393 the grounding zone (Farinotti et al., 2014). Under the assumption of mass balance equilibrium,
394 supported by the observed steady ice motion since 1995, a specific surface mass balance $b_n = 230$
395 kg m^{-2} is inferred from the ice flux across the grounding line.

396 The stable velocity in 1995 and 1999 suggests that Flask Glacier has been close to equilibrium state
397 in those years. Thus, assuming equilibrium condition, the 1995 mass flux of 0.78 Gt a^{-1} across the
398 flux gate results in $b_n = 779$ kg m^{-2}, 3.4 times higher than the specific mass balance on Starbuck

399 Glacier. The large difference in b_n can be explained by the strong west-east decrease of
400 accumulation (Turner et al., 2002). Flask Glacier flows down from the main ice divide of the
401 peninsula, whereas Starbuck Glacier originates on a small ice plateau 25 km to the east, separated
402 from the main divide by the deep trough of Crane Glacier.

403 Flask and Leppard glaciers have responded to the changing stress conditions on the ice shelf in front
404 by acceleration. The bedrock of Flask and Leppard glaciers ascends towards the grounding zone
405 from depressions several kilometres upstream (Farinotti et al., 2013; Huss and Farinotti, 2014). The
406 height of the glacier surface above the bedrock suggests that the glaciers are still firmly grounded
407 above at the flux gates. Consequently, changes in the force balance of the grounding zone probably
408 played a main role for initializing flow acceleration.

409 Scambos et al. (2014) report rates of mass change of +0.12 Gt a^{-1} for Flask Glacier and -1.31 Gt a^{-1}
410 for Leppard Glacier, based on differencing of optical stereo DEMs from November 2001 to
411 November 2006 and ICESat data from 2003 to 2008. Our analysis over recent years does not show
412 a contrasting behaviour for the two glaciers. Under assumption that the 1995 fluxes correspond to
413 the balance fluxes, we obtain for different dates between 2009 to 2013 mass change rates of -0.30
414 Gt a^{-1} to -0.44 Gt a^{-1} for Flask Glacier and -0.52 Gt a^{-1} to -0.56 Gt a^{-1} for Leppard Glacier.

415

416 **6. Conclusions**

417 The collapse of the main section of Larsen B Ice Shelf in March 2002 triggered a near immediate
418 response of most tributary glaciers with increased velocities maintained to date. Acceleration of ice
419 flow is also observed on the remnant part of the ice shelf in SCAR Inlet and its main tributaries. The
420 behaviour of the individual glaciers varies, and velocities show significant fluctuations over time.
421 Whereas, after an initial speed up, Crane and Jorum glaciers slowed down significantly since mid-
422 2007, the Hektoria and Green glaciers continue to show widespread fluctuations in velocity and
423 periods of major frontal retreat alternating with more stationary positions or short term frontal
424 advance. These differences in the response are related to glacier geometry and bedrock features.
425 Crane and Jorum glaciers retreated into deep and narrow fjords while Hektoria and Green glaciers
426 still calve into a wide bay. Temporal fluctuations of flow velocity are a main factor for fluctuations
427 in ice discharge, emphasizing the importance of common epochs for reconciling glacier mass
428 balance estimates derived by different methods (Shepherd et al., 2012).

429 Because of the combined effect of slow down and decrease in ice thickness, the ice discharge of
430 Crane Glacier decreased by 66 % between 2007 and 2013 and of Jorum Glacier by 26 %. Both
431 glaciers are expected to retreat further inland before reaching a new equilibrium in spite of slow-

down, concluding from ongoing thinning and the increase of floating ice area. Hektoria and Green glaciers maintained variable but consistently high rates of mass depletion in recent years, as the calving front alternated between floating and weakly grounded phases.

The increase of flow velocity on SCAR Inlet ice shelf and its larger tributaries started soon after the 2002 Larsen B collapse event, but changes have been discontinuous with most of the increase in the first years followed by comparatively small variations in velocity since 2009. On the smaller tributaries changes have been modest or absent. The velocity on the ice shelf section downstream of Flask and Leppard glaciers, the largest tributaries, increased two- to three fold since 1995/1999. The velocity at the flux gates of these glaciers increased until 2009 by 38 % and 44%, respectively, with minor fluctuations in velocity in later years. This suggests that the SCAR Inlet ice shelf and its main tributary glaciers may have temporarily adjusted to the loss of the backstress from the main Larsen B ice shelf. However, considering the sustained high flow velocities and the enhanced formation and extension of cracks along the shear margins of the central ice shelf section, this state will not be long-lasting. These are clear signs for flow instability that will very likely lead to a complete disintegration of SCAR Inlet Ice Shelf in the near future.

References

Berthier, E., Scambos, T.A., and Shuman, C.A.: Mass loss of Larsen B tributary glaciers (Antarctic Peninsula) unabated since 2002, Geophys. Res. Lett., 39, L13501L13501, doi:10.1029/2012GL051755, 2012.

Bindschadler, R., Vornberger, P., Fleming, A., Fox, A., Mullins, J., Binnie, D., Paulsen, S. J., Granneman, B., and Gorodetzky, D.: The Landsat Image Mosaic of Antarctica, Rem. Sens. Env., 112(12), 4214–4226, doi:10.1016/j.rse.2008.07.006, 2008.

Cook, A. J. and Vaughan, D. G.: Overview of areal changes of the ice shelves on the Antarctic Peninsula over the past 50 years, The Cryosphere, 4, 77–98, 2010.

Cook, A. J., Murray, T., Luckman, A., Vaughan, D. G., and Barrand, N. E.: A new 100-m digital elevation model of the Antarctic Peninsula derived from ASTER Global DEM: Methods and accuracy assessment, Earth Syst. Sci. Data, 4, 129–142, doi:10.5194/essd-4-129-2012, 2012.

De Angelis, H. and Skvarca, P.: Glacier surge after ice shelf collapse. Science, 299 (5612), 1560–1562. doi:10.1126/science.1077987, 2003.

Farinotti, D., Corr, H. F. J., and Gudmundsson, G. H.: The ice thickness distribution of Flask Glacier, Antarctic Peninsula, determined by combining radio-echo soundings, surface velocity data and flow modelling, Annals of Glaciology, 54 (63), doi:10.3189/2013AoG63A603, 2013.

Farinotti, D., King, E. C., Albrecht, A., Huss, M., and Gudmundsson, G. H.: The bedrock topography of Starbuck Glacier, Antarctic Peninsula, as measured by ground based radio-echo soundings, Ann. Glaciol., 55, 22–28, 2014.

Fricker, H. A. and Padman, L.: Thirty years of elevation change on Antarctic Peninsula ice shelves from multimission satellite radar altimetry, J. Geophys. Res., 117, C02026, doi:10.1029/2011JC007126, 2012.

Glasser, N. F. and Scambos, T. A.: A structural glaciological analysis of the 2002 Larsen B ice-shelf collapse, J. Glaciol., 54, 3–16, 2008.

Haran, T., Bohlander, J., Scambos, T. A., Painter, T., and Fahnestock, M.: MODIS Mosaic of Antarctica 2008-2009 (MOA2009) Image Map 2009. Boulder, Colorado USA: National Snow and Ice Data Center, http://dx.doi.org/10.7265/N5KP8037, 2014.

Hulbe, C. L., Scambos, T. A., Youngberg, T., and Lamb A. K.: Patterns of glacier response to disintegration of the Larsen B Ice Shelf, Antarctic Peninsula, Global Planet. Change, 63, 1–8, 2008.

Huss, M. and Farinotti, D.: A high-resolution bedrock map for the Antarctic Peninsula, The

16

Cryosphere, 8, 1261–1273,doi:10.5194/tc-8-1261-2014, 2014.

Jezek, K. C., Curlander, J. C., Carsey, F., Wales, C., and Barry, R.G.: RAMP AMM-1 SAR Image Mosaic of Antarctica. Version 2. Boulder, Colorado USA: National Snow and Ice Data Center, 2013.

Krabill, W. B. and Thomas, R: Pre-IceBridge ATM L2 Icessn Elevation, Slope, and Roughness. Boulder, Colorado USA: NASA DAAC at the National Snow and Ice Data Center, 2013.

Krabill, W. B. and Thomas, R: IceBridge ATM L2 Icessn Elevation, Slope, and Roughness. Version 2. Boulder, Colorado USA: NASA DAAC at the National Snow and Ice Data Center, 2014.

Krieger, G., Zink, M., Bachmann, M., Bräutigam, B., Schulze, D., Martone, M., Rizzoli, P., Steinbrecher, U., Anthony, J. W., De Zan, F., Hajnsek, I., Papathanassiou, K., Kugler, F., Rodriguez Cassola, M., Younis, M., Baumgartner, S., Lopez Dekker, P., Prats, P., and Moreira, A.: TanDEM-X: a radar interferometer with two formation flying satellites, Acta Astronaut., 89, 83–98, doi:10.1016/j.actaastro.2013.03.008, 2013.

Lavoie, C., Domack, E. W., Pettit, E. C., Scambos, T. A., Larter, R. D., Schenke, H.-W., Yoo, K. C. Gutt, J, Wellner, J., Canals, M., Anderson, J. B., and Amblas D.: Paleo-ice flow directions of the Northern Antarctic Peninsula ice sheet at LGM based upon a new synthesis of seabed imagery. The Cryosphere, 8, 613-629, 2015.

Paterson, W. S. B.: The physics of glaciers, Third Edition, Oxford, etc., Elsevier, 1994.

Rack, W.: Dynamic behaviour and disintegration of the northern Larsen Ice Shelf, Antarctic Peninsula, Ph.D. thesis, University of Innsbruck, Austria, 166 pp., 2000.

Rack, W., Doake, C. S. M., Rott, H., Siegel, A., and Skvarca, P.: Interferometric analysis of the deformation pattern of the Northern Larsen Ice Shelf, Antarctic Peninsula, compared to field measurements and numerical modeling, Ann. Glaciol., 31, 205–210, 2000.

Rack, W. and Rott, H.: Pattern of retreat and disintegration of Larsen B Ice Shelf, Antarctic Peninsula, Ann. Glaciol., 39, 505-510, 2004.

Rignot, E., Casassa, G., Gogineni, P., Rivera, A., and Thomas, R.: Accelerated ice discharges from the Antarctic Peninsula following the collapse of the Larsen B Ice Shelf. Geophys. Res. Lett., 31, L18401, doi:10.1029/2004GL020697, 2004.

Rott, H.: Advances in interferometric synthetic aperture radar (InSAR) in earth system science, Progress in Phys. Geogr., 33(6), 769-791, doi: 10.1177/0309133309350263, 2009.

Rott, H., Skvarca, P., and Nagler, T.: Rapid collapse of Northern Larsen Ice Shelf, Antarctica,

Science, 271, 788–792, 1996.

Rott, H., Rack, W., Skvarca, P., and De Angelis, H.: Northern Larsen Ice Shelf, Antarctica: Further retreat after collapse, Ann. Glaciol., 34, 277– 282, 2002.

Rott, H., Müller, F., Nagler, T., and Floricioiu, D.: The imbalance of glaciers after disintegration of Larsen B Ice Shelf, Antarctic Peninsula, The Cryosphere, 5 (1): 125–134. doi:10.5194/tc-5-125-2011, 2011.

Rott, H., Floricioiu, D., Wuite, J., Scheiblauer, S., Nagler, T., and Kern.M.: Mass changes of outlet glaciers along the Nordensjköld Coast, northern Antarctic Peninsula, based on TanDEM-X satellite measurements, Geophys. Res. Lett., 41, doi:10.1002/2014GL061613, 2014.

Scambos, T. A., Bohlander, J. A., Shuman, C. A., and Skvarca, P.: Glacier acceleration and thinning after ice shelf collapse in the Larsen B embayment, Antarctica, Geophys. Res. Lett., 31, L18402, doi:10.1029/2004GL020670, 2004.

Scambos, T. A., Berthier, E., and Shuman, C. A.: The triggering of subglacial lake drainage during rapid glacier drawdown: Crane Glacier, Antarctic Peninsula, Ann.Glaciol., 52(59), 74-82, 2011.

Scambos, T. A., Berthier, E., Haran, T., Shuman, C. A., Cook, A. J., Ligtenberg, S. R. M., and Bohlander, J.: Detailed ice loss pattern in the northern Antarctic Peninsula: widespread decline driven by ice front retreats, The Cryosphere, 8, 2135-2145, doi:10.5194/tc-8-2135-2014, 2014.

Shepherd, A., Ivins, E. R., Geruo, A, Barletta, V. R., Bentley, M. J., Bettadpur, S., Briggs, K. H., Bromwich, D. H., Forsberg, R., Galin, N., Horwath, M., Jacobs, S., Joughin, I., King, M. A., Lenaerts, J. T., Li, J., Ligtenberg, S. R., Luckman, A., Luthcke, S. B., McMillan, M., Meister, R., Milne, G., Mouginot, J., Muir, A., Nicolas, J. P., Paden, J., Payne, A. J., Pritchard, H., Rignot, E., Rott, H., Sørensen, L. S., Scambos, T. A., Scheuchl, B., Schrama, E. J., Smith, B., Sundal, A. V., van Angelen, J. H., van de Berg, W.J., van den Broeke, M. R., Vaughan, D. G., Velicogna, I., Wahr, J., Whitehouse, P. L., Wingham, D. J., Yi, D., Young, D., and Zwally, H. J.: A reconciled estimate of ice-sheet mass balance, Science, 338, 1183–1189, doi:10.1126/science.1228102, 2012.

Shuman, C. A., Berthier, E., and Scambos, T. A.: 2001–2009 elevation and mass losses in the Larsen A and B embayments, Antarctic Peninsula, J. Glaciol., 57, 737–754, 2011.

Turner, J., Lachlan-Cope, T. A., Marshall, G. J., Morris, E. M., Mulvaney, R., and Winter, W.: Spatial variability of Antarctic Peninsula net surface mass balance, J. Geophys. Res., 107(D13), 4173, doi:10.1029/2001JD000755, 2002.

Vieli, A. and Payne, A. J.: Assessing the ability of numerical ice sheet models to simulate grounding line migration, J. Geophys. Res.-Earth, 110, F01003, doi:10.1029/2004JF000202, 2005.

552 Vieli, A., Payne, A. J., Du, Z., and Shepherd, A.: Numerical modelling and data assimilation of the
553 Larsen B Ice Shelf, Antarctic Peninsula, Phil. Trans. R. Soc. A, 364, 1815–1839,
554 doi:10.1098/rsta.2006.1800, 006, 2006.

555 Zgur, F., Rebesco, M., Domack, E. W., Leventer, A., Brachfeld, S., and Willmott, V.: Geophysical
556 survey of the thick, expanded sedimentary fill of the new-born Crane fjord (former Larsen B Ice
557 Shelf, Antarctica): in Antarctica: A Keystone in a Changing World – Online Proceedings of the 10th
558 ISAES, edited by: Cooper, A., Raymond, C., and the 10th ISAES Editorial Team, USGS Open-File
559 Report 2007–1047, Extended Abstract 141, p. 4 p., 2007.

560

561 **Tables**

562 **Table 1**. Area of glacier basins (in km^2) shown in Fig. 1 above the October 1995 grounding line and

563 updated for glacier fronts on 12 January 2012, and change of glacier area 1995 to 2012. NC – no

564 significant change of front position or grounding line. The areas of glacier basins include rock

565 outcrops and mountain slopes.

Nr.	Glacier	Area (km^2) 10/1995	Area (km^2) 01/2012	ΔArea (km^2) 1995-2012
1	Hektoria Glacier Headland	118.13	100.64	-17.49
2	HGE	1588.97	1415.05	-173.92
3	Evans Glacier Headland	124.38	119.49	-4.89
4	Punchbowl	129.56	117.82	-11.74
5	Jorum	484.09	460.36	-23.73
6	Crane	1354.29	1319.74	-34.55
7	Mapple	154.97	155.43	+0.46
8	Melville	295.26	291.18	-4.08
9	Pequod	151.06	150.64	-0.42
10	Rachel	51.27	51.27	NC
11	Starbuck	300.69	300.69	NC
12	Stubb	109.92	109.92	NC
13	Flask	1144.84	1144.84	NC
14	Leppard	1877.08	1877.08	NC
Sum		*7884.51*	*7614.15*	*-270.36*

566

567

568 **Table 2.** Drainage area above the flux gate, velocities at the centre of the flux gate (V_c), discharge

569 across the flux gates, and difference of discharge versus 1995; for glaciers draining into Larsen B

570 embayment. * From Rott et al. (2011).

571

Glacier	Gate	Area km^2	Date YYYY-MM	V_c (m a^{-1})	Discharge (Gt a^{-1})	Δ1995-Date 2 (Gt a^{-1})
Crane	C1	1235	1995/99*	548	1.15 ±0.13	
			2007-06	2464	5.02 ±0.56	-3.87
			2008/09*	1882	2.92 ±0.33	-1.77
			2010-04	1650	2.44 ±0.27	-1.29
			2011-01	1329	2.21 ±0.25	-1.06
			2012-08	1292	2.15 ±0.24	-1.00
			2013-11	1059	1.72 ±0.19	-0.57
Jorum	J1	382	1995/99*	475	0.35 ±0.07	
			2008/09*	865	0.53 ±0.11	-0.18
			2012-04	759	0.39 ±0.08	-0.04
	J2	52	1995/99*	68	0.04 ±0.02	
			2008/09*	146	0.08 ±0.02	-0.04
			2012-04	153	0.06 ±0.01	-0.02
Hektoria -Green	H1 & G1	1188	1995/99*	387	1.19 ±0.25	
			2004-03	1862	4.74 ±0.98	-3.55
			2008/09*	1545	2.88 ±0.59	-1.69
Hektoria	H2	341	2010-11	822	1.67 ±0.34	
			2013-07	741	1.49 ±0.31	
Green	G2	618	2010-11	1278	1.99 ±0.41	
			2013-07	1095	1.56 ±0.31	

572

573

574   **Table 3 .**Drainage area above the flux gate, velocities at the centre of the flux gate (V_c), discharge

575   across the flux gates, and difference of discharge versus 1995; for glaciers draining into SCAR Inlet

576   ice shelf.

577

Glacier	Area (km^2)	Date (YYYY-MM)	V_c (m a^{-1})	Discharge (Gt a^{-1})	Δ1995-Date 2 (Gt a^{-1})
Starbuck	296	1995-10	124	0.07 ±0.01	
		2009-09	125	0.07 ±0.01	
		2011-01	124	0.07 ±0.01	
Flask	1003	1995-10	478	0.78 ±0.09	
		1999-11	496	0. 80 ±0.09	
		2009-09	661	1.11 ±0.12	-0.33
		2011-01	704	1.23 ±0.14	-0.45
		2012-02	690	1.15 ±0.13	-0.37
		2013-07	642	1.08 ±0.12	-0.30
Leppard	1822	1995-10	365	1.22 ±0.25	
		2009-10	526	1.74 ±0.36	-0.52
		2013-07	541	1.78 ±0.37	-0.565

578

579

580

Figures
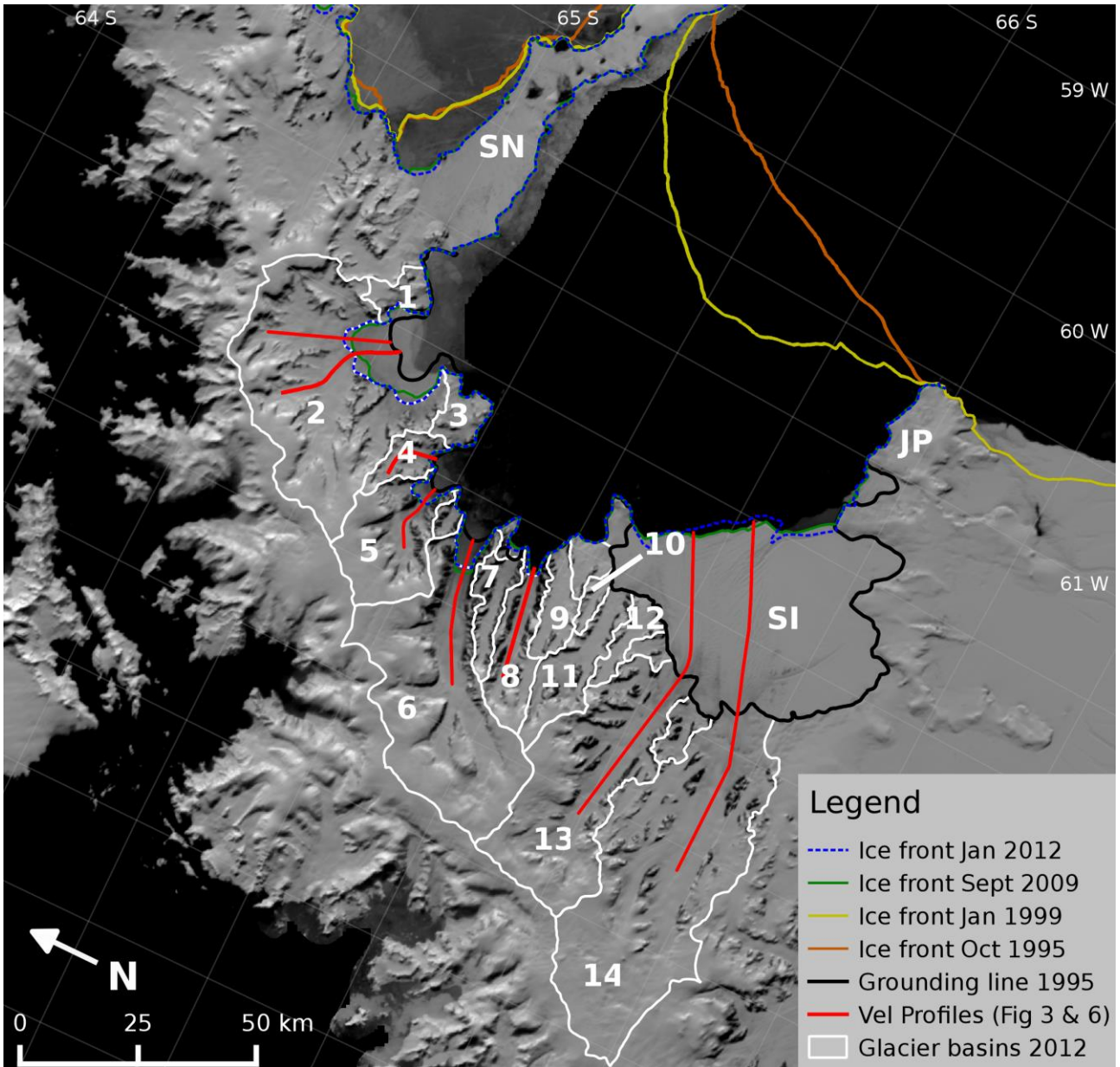
Fig. 1. Overview map of glacier basins in the Larsen B region. Background: 2009 MODIS mosaic (Haran et al., 2014). Names and size of basins in Table 1. Glacier boundaries inland are based on the ASTER GDEM (courtesy A. Cook). Coastlines and grounding line derived from ERS-1 and Landsat images. SN - Seal Nunataks, SI - SCAR Inlet, JP - Jason Peninsula. Red lines show location of velocity profiles in Figs. 3 and 6.
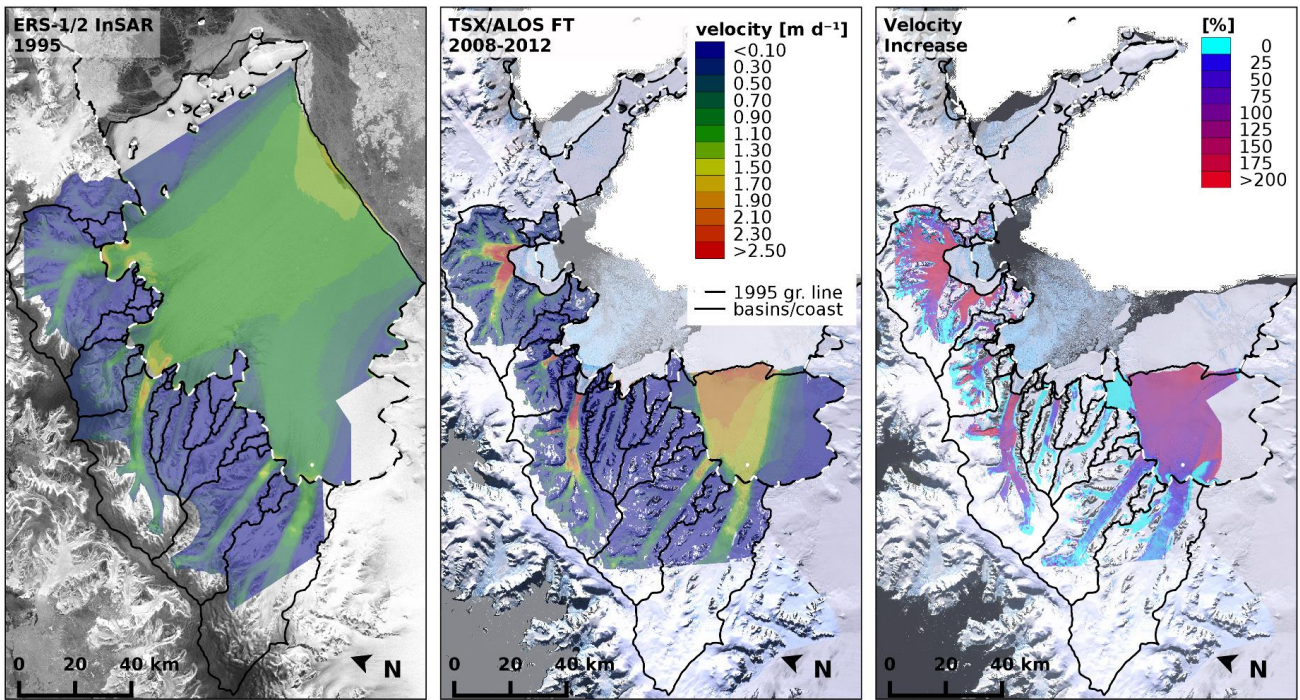
Fig. 2. Maps of glacier surface velocity in the Larsen B region. Left: based on ERS InSAR data of October/November 1995 (background RAMP mosaic; Jezek et al., 2013). Centre: based on TSX and PALSAR offset tracking 2008 – 2012. Right: Velocity increase 2008-2012 versus 1995. Background LIMA mosaic (Bindschadler et al., 2008). The dashed line shows the position of the 1995 grounding line. Front positions are from October 1995 (left) and January 2012 (center and right).
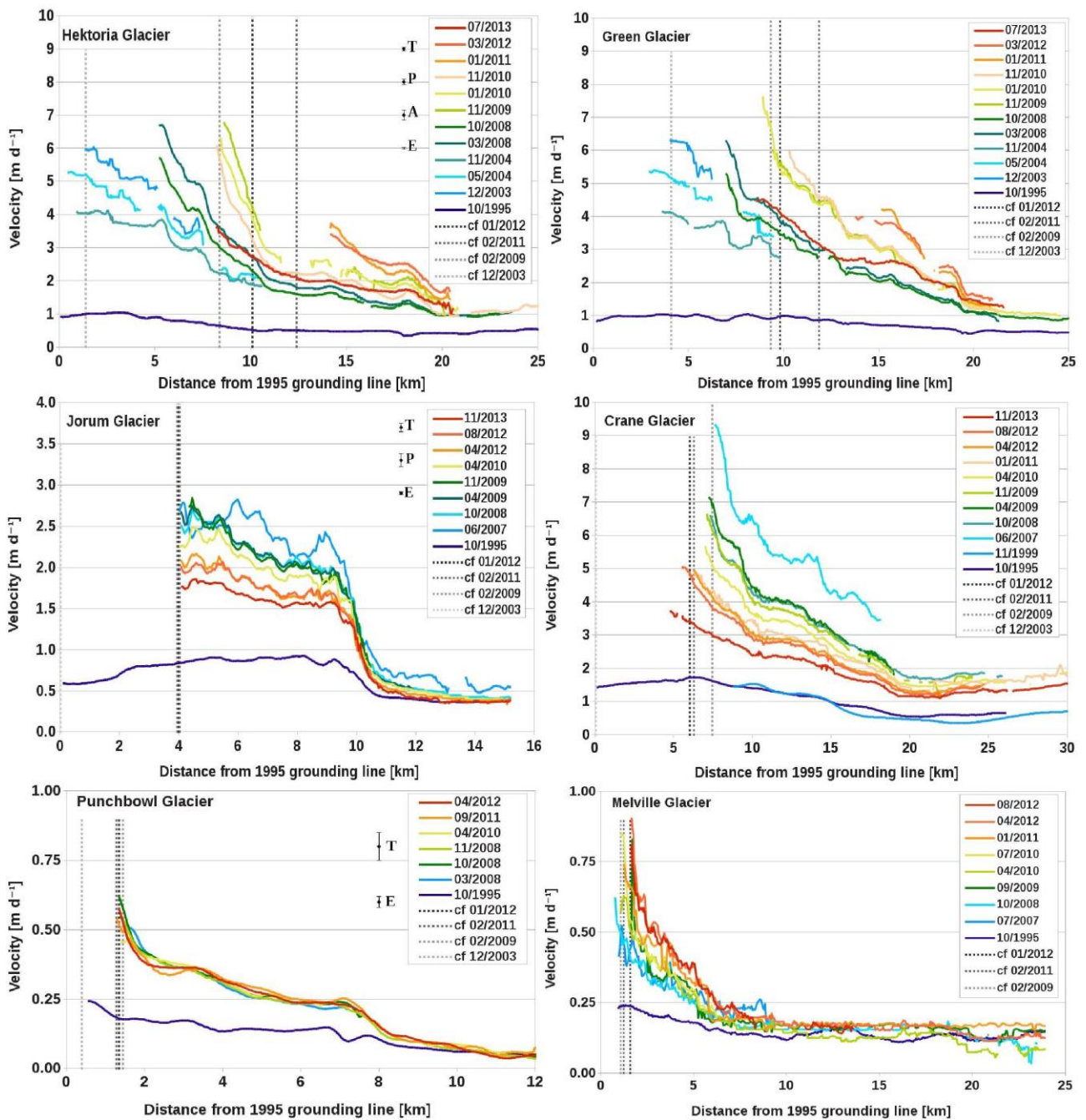
Fig. 3. Surface velocities along the central flow line of Hektoria, Green, Jorum, Crane, Punchbowl and Melville glaciers and their frontal positions at different dates (month/year). The x- and y-scales are different for individual glaciers. Vertical lines show positions of calving front. The vertical bars show uncertainties in velocity for TerraSAR-X (T) 2007 to 2013; PALSAR (P), Nov. 2009; ASAR (A) 2003, 2004; ERS (E) 1995, 1999.
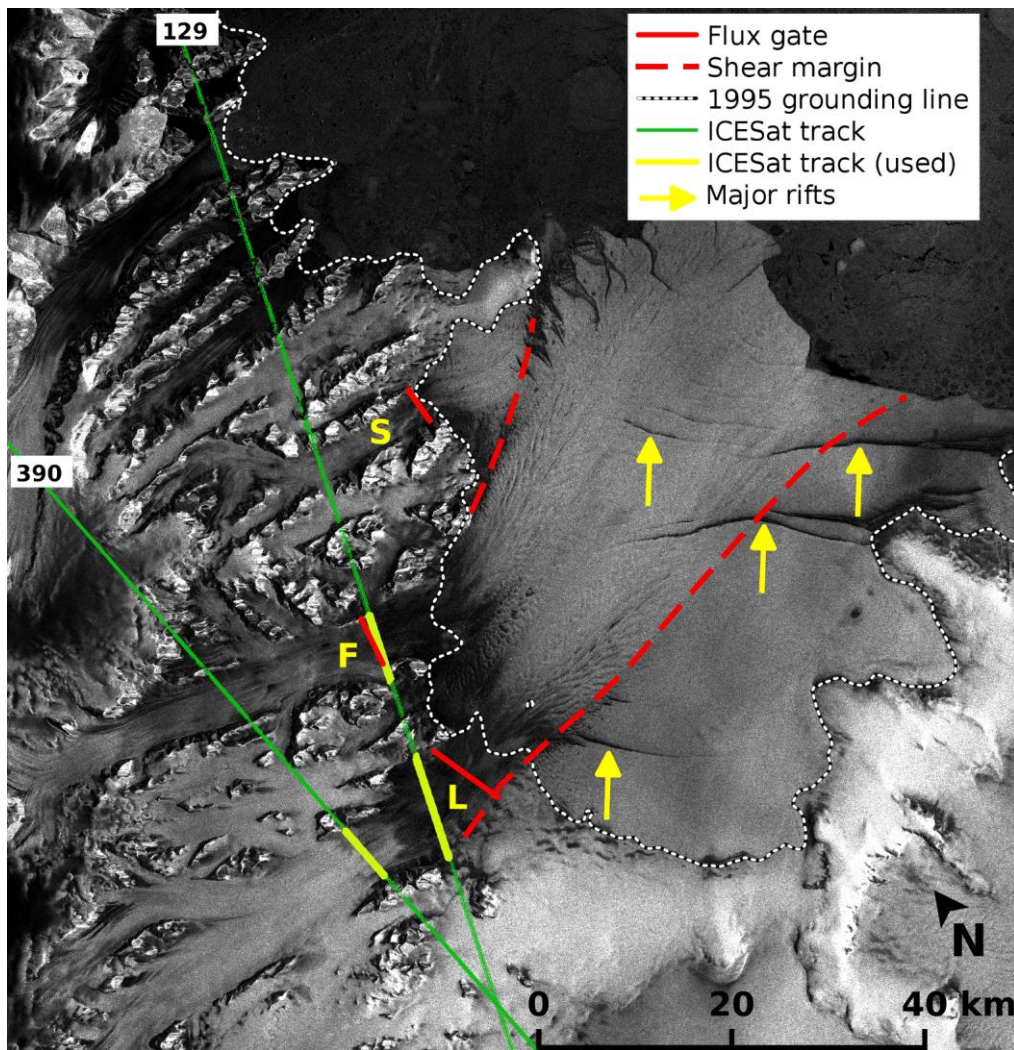
607

608

609
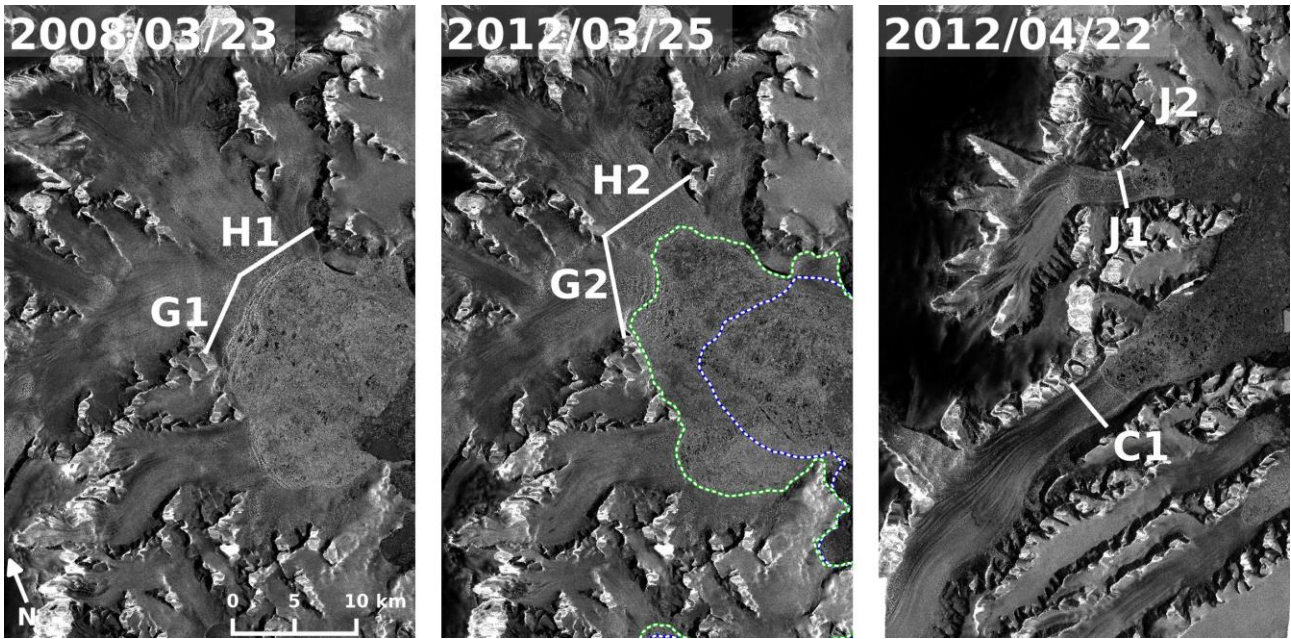
Fig. 4. Section of TerraSAR-X amplitude images. Left and Center: HGE glaciers on 23 March 2008 and 25 March 2012, with flux gates on Hektoria (H) and Green (G) glaciers and location of the glacier front on 24 December 2004 (dotted blue line) and 25 March 2012 (dotted green line). Right: TSX image of Crane (C) and Jorum (J) glaciers on 22 April 2012 with flux gates.

Fig. 5. Envisat ASAR image of SCAR Inlet ice shelf and tributary glaciers, 28 January 2004. Red lines show the flux gates for Flask (F), Leppard (L) and Starbuck (S) glaciers. The broken red lines delimit the outflow downstream of Flask and Leppard glaciers. The yellow sections of the ICESat tracks are used for deriving surface elevation change on Leppard and Flask glaciers. The arrows point to major rifts.
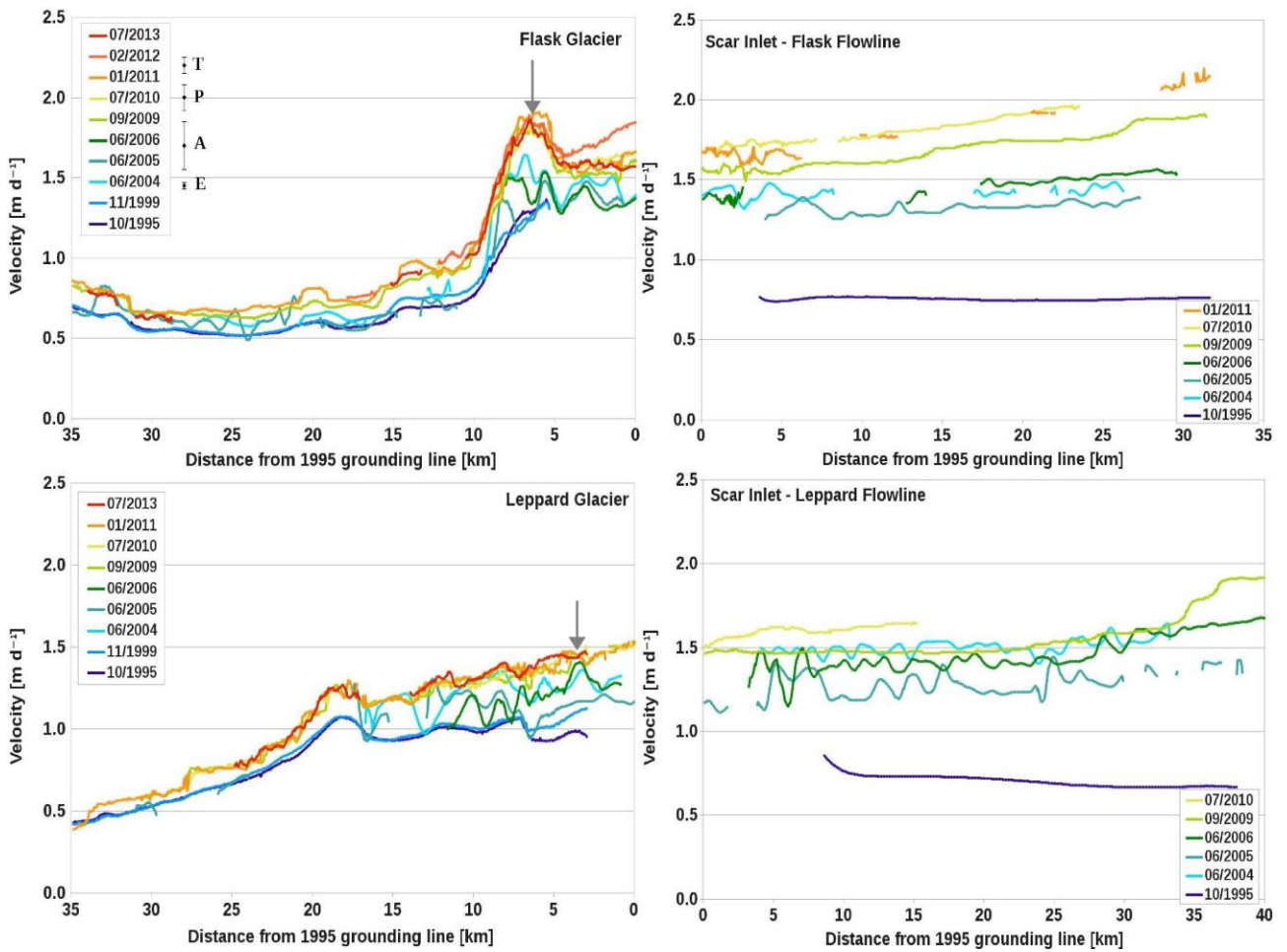
Fig. 6. Surface velocities along the central flowline of Flask (top left) and Leppard (bottom left) glaciers and downstream of these glaciers on SCAR Inlet ice shelf (right, top and bottom). Different y-scale for Leppard Flowline. The arrow shows the location of the flux gate. Position of flowline profiles shown in Fig.1 and of flux gates in Fig. 5. The vertical bars show uncertainties in velocity for TerraSAR-X (T) 2007 to 2013; PALSAR (P) Nov. 2009; ASAR (A) 2003, 2004; ERS (E) 1995, 1999.

28

629
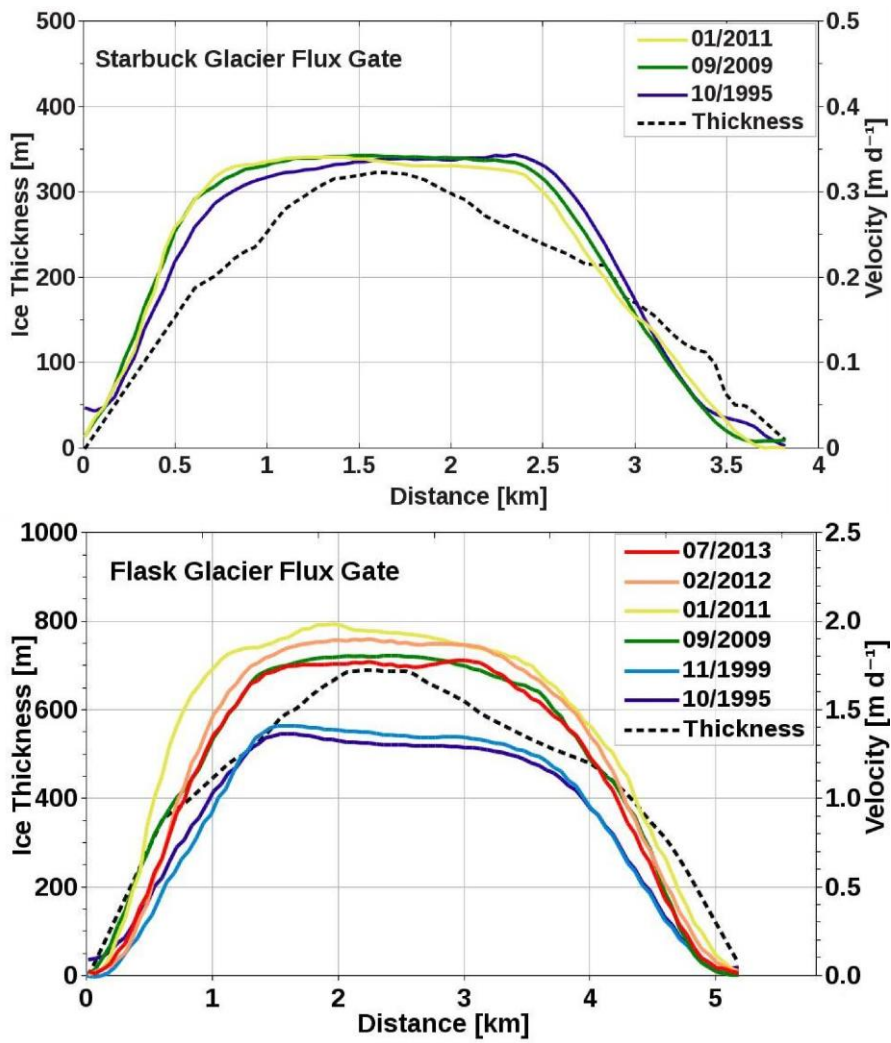
Fig. 7. Ice thickness and surface velocity across the flux gate of Starbuck Glacier (top) and Flask Glacier (bottom). Ice thickness from Farinotti et al. (2013; 2014).

630
631
632